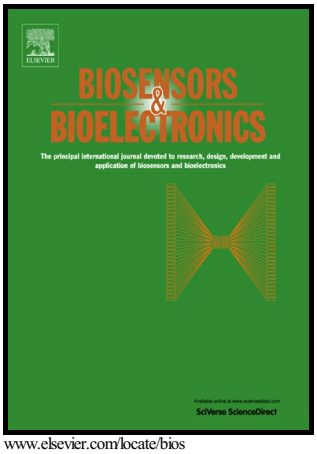

www.elsevier.com/locate/bios

An Electrochemical Biosensor Based on the Enhanced Quasi-Reversible Redox Signal of Prussian Blue Generated by Self-Sacrificial Label of Iron Metal-Organic Framework

Lin Cui, Juan Hu, Chen-chen Li, Cheng-ming Wang, Chun-yang Zhang

PII: S0956-5663(18)30753-X
DOI: https://doi.org/10.1016/j.bios.2018.09.061
Reference: BIOS10801

To appear in: *Biosensors and Bioelectronic*

Received date: 9 July 2018
Revised date: 15 September 2018
Accepted date: 17 September 2018

Cite this article as: Lin Cui, Juan Hu, Chen-chen Li, Cheng-ming Wang and Chun-yang Zhang, An Electrochemical Biosensor Based on the Enhanced Quasi-Reversible Redox Signal of Prussian Blue Generated by Self-Sacrificial Label of Iron Metal-Organic Framework, *Biosensors and Bioelectronic,* https://doi.org/10.1016/j.bios.2018.09.061

An Electrochemical Biosensor Based on the Enhanced Quasi-Reversible Redox Signal of Prussian Blue Generated by Self-Sacrificial Label of Iron Metal-Organic Framework

Lin Cui,† Juan Hu,† Chen-chen Li,† Cheng-ming Wang, and Chun-yang Zhang*

College of Chemistry, Chemical Engineering and Materials Science, Collaborative Innovation Center of Functionalized Probes for Chemical Imaging in Universities of Shandong, Key Laboratory of Molecular and Nano Probes, Ministry of Education, Shandong Provincial Key Laboratory of Clean Production of Fine Chemicals, Shandong Normal University, Jinan 250014, PR China.

Abstract

We develop for the first time a new electrochemical biosensor for signal-on detection of T4 polynucleotide kinase (PNK) based on the enhanced quasi-reversible redox signal of prussian blue generated by self-sacrificial label of iron metal-organic framework (FeMOF). The DNA hairpin probe modified with FeMOF@AuNPs at the 3'-thiol end acts as the substrate of PNK. The presence of PNK enables the 5'-phosphorylation of hairpin probe, which may subsequently function as the substrate of lambda exonuclease. Lambda exonuclease removes the 5' mononucleotides from the stem, unfolding the hairpin structure and releasing the single-stranded DNA (ssDNA). The resultant FeMOF@AuNP-modified ssDNA may specifically hybridize with the capture probe to form the double-strand DNA (dsDNA) duplex, enabling the immobilization of FeMOF on the electrode surface. The reaction of Fe^{3+} in the MOF with $K_4Fe(CN)_6$ leads to the formation of prussian blue on the electrode surface and consequently the generation of a high electrochemical signal. This assay is very simple without the involvement of the pre-synthesized prussian

blue which is unstable in neutral buffer, and the self-sacrificial label of FeMOF can achieve great signal amplification without the involvement of any extra functional materials. Due to the introduction of self-sacrificial label of FeMOF and the formation of prussian blue nanolayers with good quasi-reversible cyclic voltammetric electrochemical activity, this biosensor exhibits high sensitivity and a large dynamic range. Moreover, this biosensor can be used to screen the PNK inhibitors, holding great potential in disease diagnosis and drug discovery.

Keywords: Electrochemical biosensor; Quasi-Reversible; Prussian Blue; Self-Sacrificial Label; Iron Metal-Organic Framework

*Tel.: +86 0531-86186033. Fax: +86 0531-82615258. E-mail: cyzhang@sdnu.edu.cn.

.

1. Introduction

Metal-organic frameworks (MOFs) are crystalline molecular materials which consist of metal ions or clusters connected by organic linker groups. The structures of MOFs are versatile and controllable by architecture design and pore functionalization (Furukawa et al. 2013). Owing to their distinctive features of high pore volumes, large surface areas, multiple topologies, tunable pore size and surface chemistry, MOFs have been widely used in the adsorption and separation (Cui et al. 2014; McKinlay et al. 2013), sensing (Cui et al. 2015b; Jiang et al. 2015; Shen et al. 2015), catalysis (Horcajada et al. 2007; Liu et al. 2014) and drug delivery (Orellana-Tavra et al. 2015). Among the plentiful transition metal ions that are able to build up MOFs, iron ion (Fe^{3+}) is an environmentally benign and cheap component with non-toxicity and redox properties. Fe-based MOFs (e.g.PCN-222 with porphyrinic Fe(III) center (Feng et al. 2012), Fe(III)-based MIL-53 (the MIL stands for the materials from Institut Lavoisier) (Ai et al. 2013), MIL-68 and MIL-100 (Zhang et al. 2014) and MIL-88

(Liu et al. 2013) have demonstrated the intrinsic peroxidase-like oxidation reaction activity for colorimetric assay, but few FeMOF-based electrochemical biosensors are reported so far despite the excellent stability and redox activity of FeMOF.

As the typical MOF materials, prussian blue analogues are the prototypes of transition-metal hexacyanometalates with a face-centered cubic lattice containing an open, zeolite-like structure. Prussian blue analogues consist of alternating ferric and ferrous ions which are bridged by organic cyanide ions. Prussian blue may provide facile assembly and precise interaction with active sites at functional interfaces for sensing and biomedical applications (Chen et al. 2017; Cui et al. 2015a; Kong et al. 2015; Su et al. 2016). Especially, prussian blue is often used as an efficient mediator and nanoenzyme in electrochemical sensors due to its high electrochemical/electrocatalytic properties and low redox potential. As an inorganic conductive film, the prussian blue film can replace electronic media to directly produce electrochemical signal (Li et al. 2012). Recently, prussian blue and its derivatives have been applied for the detection of hydrogen peroxide (Cui et al. 2015a; Su et al. 2017), nitrite (Cui et al. 2012), oxytetracycline (Li et al. 2012) adenosine triphosphate (Wang et al. 2018), organophosphorous pesticides (Li et al. 2014b), and antigen (Lai et al. 2009). However, the hydrolysis of prussian blue in neutral/alkaline solution may decrease the electrochemical signal, greatly limiting the use of the pre-synthesized prussian blue in biosensor development (Ricci et al. 2003).

A typical cyclic voltammetric curve of prussian blue-based electrochemical interfaces consists of two sets of peaks (Kong et al. 2015). The response at negative potential (~0.2 V vs. Ag/AgCl) corresponds to the reduction/oxidation of a high-spin system $Fe^{3+/2+}$, while the other couple at positive potentials (~1.0 V vs. Ag/AgCl) results from the redox reaction of low spin $Fe(CN)_6^{3-/4-}$. Among the two reversible

redox reactions, the reversible redox response to $Fe^{3+/2+}$ is more widely used due to the decrease of oxygen absorption. Prussian blue has been reported as an artificial peroxidase with excellent electrocatalytic reduction capability towards H_2O_2 (Su et al. 2017), but few reports are about the development of prussian blue-based electrochemical sensor with cyclic voltammetry.

Polynucleotide kinase (PNK) can catalyze the phosphorylation of nucleic acids with 5′-hydroxyl termini, and plays critical roles in the DNA repair in response to various damages such as single-strand break, base excision, and oxidative DNA damage (Breslin and Caldecott 2009; Whitehouse et al. 2001; Wiederhold et al. 2004). In addition, the human PNK participates in the maintenance of genetic integrity (Li et al. 2014a; Rasouli-Nia et al. 2004) and is closely associated with various human diseases such as Werner syndrome, Rothmund Thomson syndrome and Bloom's syndrome (Brosh and Bohr 2007; Sharma et al. 2006). Consequently, it is of great importance to develop sensitive methods for PNK assay. The electrochemical method has distinct advantages of low cost, portability and high sensitivity (Cui et al. 2015b; Li. et al., 2017; Wang et al., 2014; Yin et al., 2015). Herein, we develop for the first time a new electrochemical biosensor for signal-on detection of T4 PNK based on the enhanced quasi-reversible redox signal of prussian blue generated by self-sacrificial label of FeMOF. The self-sacrificial template method is an important approach for constructing the shapes of various materials by etching the templates. A typical example is the use of MOFs as the precursor self-sacrificial frameworks to fabricate the porous metal oxides (Bi et al. 2012; Ding et al. 2016; Sarkar et al. 2014; Zhou et al. 2017; Zou et al. 2014). In this research, we employed the DNA hairpin probe modified with FeMOF@AuNPs at the 3’-thiol end as the substrate of PNK. The presence of PNK results in the FeMOF@AuNP-modified ssDNA which may

specifically hybridize with the capture probe to form the dsDNA duplex, enabling the immobilization of FeMOF on the electrode surface. The reaction of Fe^{3+} in the FeMOF with $K_4Fe(CN)_6$ and H^+ leads to the formation of prussian blue on the electrode surface and consequently the generation of a high electrochemical signal. This assay is very simple without the involvement of the pre-synthesis of prussian blue which is unstable in neutral buffer, and the self-sacrificial label of FeMOF can achieve great signal amplification without the involvement of any extra functional materials.

2. Materials and methods

2.1. Materials and reagents

Potassium hexacyanoferrate (II) trihydrate ($K_4Fe(CN)_6 \cdot 3H_2O$), hydrochloric acid (HCl), and potassium chloride (KCl) were purchased from Sinopharm Chemical Reagent Co., Ltd. (Beijing, China). Hydrogen tetrachloroaurate ($HAuCl_4 \cdot 4H_2O$), 2-aminoterephthalic acid, bovine serum albumin (BSA), lysozyme, adenosine triphosphate (ATP), adenosine diphosphate (ADP), tris(hydroxymethyl)aminomethane and mercaptohexanol (MCH) were obtained from Sigma-Aldrich Chemical Co. (St. Louis, MO, USA). T4 polynucleotide kinase (10 U μL^{-1}), lambda exonuclease (5 U μL^{-1}), T4 DNA ligase, *E.coli* ligase and protein kinase A (PKA) were bought from New England Biolabs (NEB, UK). All aqueous solutions were prepared using ultrapure water obtained from a Millipore water purification system (≥18 MΩ, Milli-Q, Millipore, USA). All oligonucleotides (**Supplementary information, Table S1**) were synthesized and purified with HPLC by Takara Biotech. Co. Ltd. (Dalian, China). Human cervical carcinoma cell line (HeLa cells) was purchased from Cell

Bank, Shanghai Institutes for Biological Sciences, Chinese Academy of Sciences (Shanghai, China).

2.2. Apparatus

All electrochemical measurements were carried out on a CHI 660e electrochemical workstation (CH Instruments Inc., USA) at room temperature with a conventional three-electrode system composed of a platinum wire, a saturated calomel and a glass carbon electrode (d = 3 mm) as the counter, reference and working electrodes, respectively. Cyclic voltammetry (CV) measurements were carried out in scanning potential from -0.2 to 0.6 V in solution containing 0.1 M HCl and 0.1 M KCl. Electrochemical impedance spectroscopic (EIS) measurements were performed in 0.1 M KCl containing 5 mM $[Fe(CN)_6]^{3-}$/$[Fe(CN)_6]^{4-}$over a frequency range from 10 kHz to 0.1 Hz using an alternative voltage with an amplitude of 10 mV, superimposed on a dc potential of 0.20 V (vs SCE). Scanning electron microscopic (SEM) images were collected on a Sirion-100 (FEI) and a SU-8010 (Hitachi) scanning electronic microscope. Powder X-ray diffraction (XRD) patterns were measured at a Rigaku D/MAX 2200PC X-ray diffractometer (Japan) with Cu K_α radiation (λ = 0.154178 nm, graphite monochromator, 28 kV and 20 mA). Zeta potential was measured with a Malvern Zeta Sizer Nano (Malvern Instruments). The chemical composition was analyzed by a Genesis 2000 Energy-Dispersive X-ray Spectrometer (EDX) with SUTW-Sapphire Detector at 20 kV.

2.3. Synthesis of FeMOF and FeMOF@AuNPs-hairpin probe

FeMOF was prepared according to previous report with some modification (Liu et al. 2013). Briefly, 0.126 g (0.692 mmol) of 2-aminoterephthalic acid and 0.187 g (0.692 mmol) of $FeCl_3 \cdot 6H_2O$ were dissolved in 15 mL of DMF, and then 3.45 mmol

of acetic acid was added into the mixture solution. The mixture solution was placed in an oil bath at 120 ^{o}C for 4 h for crystallization. After cooling to room temperature, the particles were isolated by centrifugation, and washed with DMF and ethanol to remove the excess reactants, followed by drying in a vacuum oven. For the synthesis of AuNPs, 100 mL of 0.01% $HAuCl_4$ solution was boiled with vigorous stirring, followed by quick addition of 2.5 mL of 1% trisodium citrate solution. When the AuNPs were formed, the solution turned deep red, followed by stirring and cooling down.

The FeMOF containing NH_2 group was modified with AuNPs by mixing 4 mL of AuNPs (13 nm diameter) solution (Ambrosi et al. 2007) with 2 mL of 1 mg mL^{-1} FeMOF and shaking vigorously for 2 h. The obtained FeMOF@AuNPs composite was collected by centrifugation, washing with ultrapure water for three times, and dispersion in 1 mL of 10 mM Tris-HCl (pH 7.4). The hairpin probes were diluted to 1 μM and incubated in the solution containing 10 mM Tris-HCl (pH 7.4) and 1.5 mM $MgCl_2$ for 4 min at 95 °C for denaturation, followed by cooling to the room temperature to enable the formation of hairpin structure. At last, 200 μL of 2 μM hairpin probe was added in the FeMOF@AuNPs solution by stirring for 12 h at 4 °C, and then the hairpin probe-labeled FeMOF@AuNPs (FeMOF@AuNPs-hairpin probes) were obtained by the interaction of the AuNPs with the NH_2 group of hairpin probe.

2.4. Fabrication of Electrochemical Sensing Platform

Prior to the modification, the GC electrode was polished to a mirror-like surface with 1.0, 0.3 and 0.05 μm α-Al_2O_3 slurry, respectively, followed by successive sonication with ethanol and ultrapure water for 3 min to remove the residual alumina powder. After drying in a nitrogen stream, 10 μL of 0.05 mg mL^{-1} chitosan and AuNPs solution were sequentially dropped on the working electrode. After the

evaporation of solvent, the electrode surface was thoroughly rinsed with the redistilled deionized water and dried in air. Then the electrode was incubated with 6 μL of 0.5 μM capture probe containing 25 μM TCEP (the TCEP was used to reduce the disulfide bonded oligonucleotides) at room temperature for 12 h to make capture probe immobilize onto the surface of gold nanoparticles via gold-sulfur chemistry. After the electrode was thoroughly rinsed with 10 mM PBS (pH 7.4) and dried under a stream of nitrogen gas, 6 μL of 1 mM MCH was dropped on the electrode and incubated for 30 min to block the unmodified sites, followed by rinsing thoroughly with 10 mM PBS (pH 7.4) and stored at 4 °C prior to use.

2.4. Electrochemical Detection of PNK

The 2.5 μL of FeMOF@AuNPs-hairpin probe was added to the phosphorylation reaction solution (50 μL) consisting of various-concentration PNK, 0.7 mM ATP and 5 μL of 10× T4 polynucleotide kinase reaction buffer, and incubated at 37 °C for 30 min. After phosphorylation reaction, 10 U of lambda exonuclease and 5 μL of 10 × lambda exonuclease reaction buffer were added into the reaction solution and incubated at 37 °C for 30 min to perform the lambda exonuclease cleavage reaction. The biosensor was transferred to the solution containing 0.7 mM $K_3Fe(CN)_6$ and 0.1 M KCl for 15 min. Finally, cyclic voltammetry was measured in solution containing 0.1 M HCl and 0.1 M KCl to obtain the peak current.

2.5. Inhibition Assay

The ADP, NaH_2PO_4 and $(NH_4)_2SO_4$ were used as the model inhibitors. Similar procedures for PNK assay were employed for PNK inhibition assay except that the inhibitors at various concentrations were pre-mixed with the reaction buffer containing 1 U mL^{-1} PNK.

2.6. Detection of PNK activity in Cell Extracts

The HeLa cells were cultured in Dulbecco's modified Eagle's medium (DMEM) (gibco, USA) supplemented with 10% fetal bovine serum (BSA, gibco, USA) and 1% penicillin-streptomycin (gibco, USA) in 5% CO_2 incubator at 37 °C. HeLa cells were collected with trypsinization in the exponential phase of growth, washed twice with 0.1 M PBS, and centrifuged at 2000 rpm for 10 min at 4 °C. Then the cells were suspended in 100 μL of lysis buffer (10 nM Tris-HCl, pH 8.0, 150 mM NaCl, 1% NP-40, 0.25 mM sodium deoxycholate, 1.0% glycerol and 0.1 mM 4-(2-aminoethyl) benzenesulfonyl fluoride hydrochloride), incubated on ice for 30 min to thoroughly lyse the cells, followed by centrifugation at 12000 rpm for 20 min at 4 °C. The supernatant was frozen and stored at -80 °C. The 1% (v/v) cell extracts were added in the reaction buffer and subjected to the measurement of PNK activity with same procedures described above.

3. Results and discussion

3.1. Principle of PNK Assay

The principle of electrochemical biosensor for signal-on detection of PNK is shown in **Scheme 1**. We designed two DNA probes including a capture probe and a hairpin probe. The hairpin probe contains a thiol group at the 3' end for anchoring on the FeMOF@AuNPs surface and a hydroxyl group at the 5' end for PNK-actuated phosphorylation reaction. The 3' end stem of hairpin probe is partially complementary to the capture probe, and the loop structure of hairpin probe is designed to prevent the 3' end stem from being cleaved by lambda exonuclease. The capture probe contains a thiol group at the 3' end for anchoring on the surface of chitosan- and

AuNPs-modified GCE. The presence of PNK catalyzes the transfer of phosphate residue from adenosine triphosphate (ATP) to the 5'-hydroxyl end, generating a phosphorylated FeMOF@AuNPs-hairpin probe conjugate. The resultant phosphorylated hairpin probe may function as the substrate of lambda exonuclease, resulting in the stepwise removal of mononucleotides from the 5'-termini of the stem and the release of single-stranded DNA (ssDNA). The released ssDNA is partially complementary to the capture probe and may form the FeMOF@AuNPs-ssDNA/capture probe structure on the electrode surface. With the addition of $K_4Fe(CN)_6$ and acid (H^+) on the electrode surface, they react with Fe^{3+} from the FeMOF to form the electrochemically active prussian blue (ferrous ferrocyanide, $[Fe^{III}Fe^{II}(CN)_6]^-$), generating a pair of large peak current from $Fe^{3+}/^{2+}$. In the absence of PNK, the hairpin probe with a 5' hydroxyl terminus is lambda exonuclease-resistant, and the FeMOF@AuNPs-hairpin probe cannot be captured on the electrode surface without the production of electroactive prussian blue. As a result, negligible current is observed.

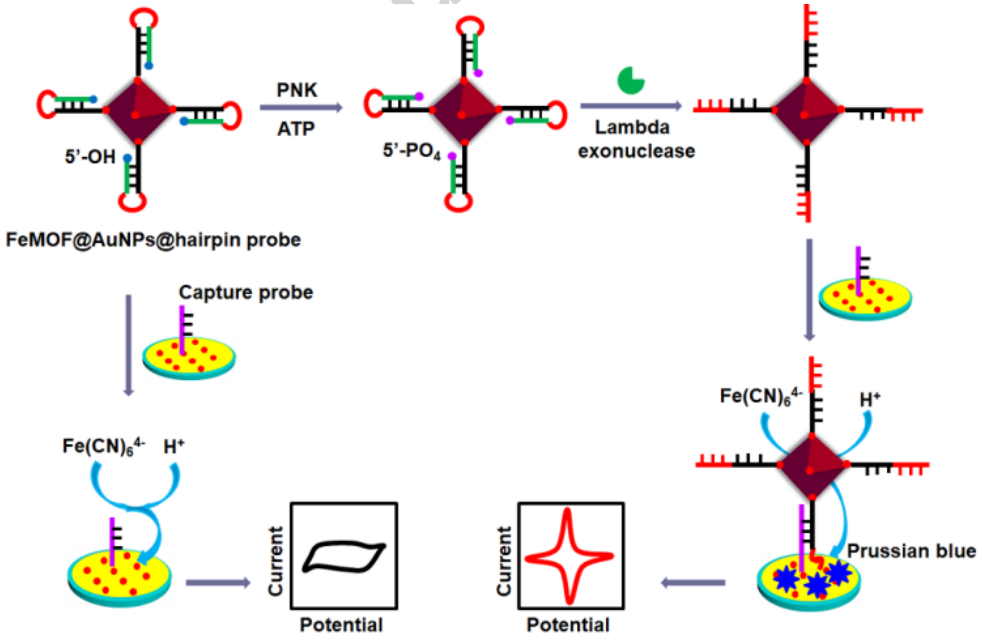

Scheme 1. Schematic illustration of an electrochemical biosensor for PNK assay based on the enhanced quasi-reversible redox signal of prussian blue generated by self-sacrificial label of FeMOF.

3.2. Characteristics of FeMOF and FeMOF@AuNPs

The crystal structure of the synthesized FeMOF is characterized by power X-ray diffraction (XRD) pattern (**Fig. 1A**). The main diffraction peaks of FeMOF (**Fig. 1A, curve a**) are observed at 9.06°, 9.98°, 16.46° and 18.88°, which correspond to the (002), (101), (200), and (201) planes at low angles, respectively, consistent with the previous report (Taylor-Pashow et al. 2009), indicating the highly crystalline of FeMOF with same structure as MIL-88 (Cr) (Surble et al. 2006). The powder XRD pattern of typical AuNPs (**Fig. 1A, curve b**) is investigated as well. The peaks at 38.2^{o}, 44.4^{o}, 64.5^{o}, and 77.5^{o} correspond to the planes of (111), (200), (220), and (311) (JCPDS: 04-0784), respectively. The diffraction peaks of both FeMOF and AuNPs are observed (**Fig. 1A, curve c**), suggesting that the successful modification of FeMOF with AuNPs. The morphologies of the synthesized nanomaterials are further characterized by scanning electron microscopy (SEM). Most of the particles in FeMOF show unusual octahedron morphology with an average diameter of 200 nm (**Fig. 1B**). In addition, the obtained FeMOF is very pure without any background signal. When AuNPs are modified on the FeMOF, AuNPs are well dispersed on the surface of FeMOF matrix (**Fig. 1C**), indicating that AuNPs are successfully adsorbed onto the FeMOF by chemical adsorption between the AuNP and the NH_2 group of FeMOF. The elemental analysis of the FeMOF and FeMOF@AuNPs is obtained by energy-dispersive X-ray spectroscopy (**Supplementary information, Fig. S1**). The

zeta potential is measured to validate the linking of AuNPs to FeMOF. The zeta potential of FeMOF in PBS (pH 7.4) is 11.2 ± 0.5 mV, facilitating its electrostatic interaction with the negatively charged citrate-capped AuNPs. The reversed zeta potential of -1.85 ± 0.4 mV indicates the successful coating of AuNPs onto the FeMOF surface. Since the FeMOF may act as the template to increase the porosity, the prussian blue film prepared from the FeMOF@AuNPs shows porous structure (**Fig. 1D**). The porous structure of prussian blue ($KFe^{III}Fe^{II}(CN)_6$) may increase the effective surface area and the mass-transfer efficiency, enhancing the electrochemical activity (Zhang et al. 2017).

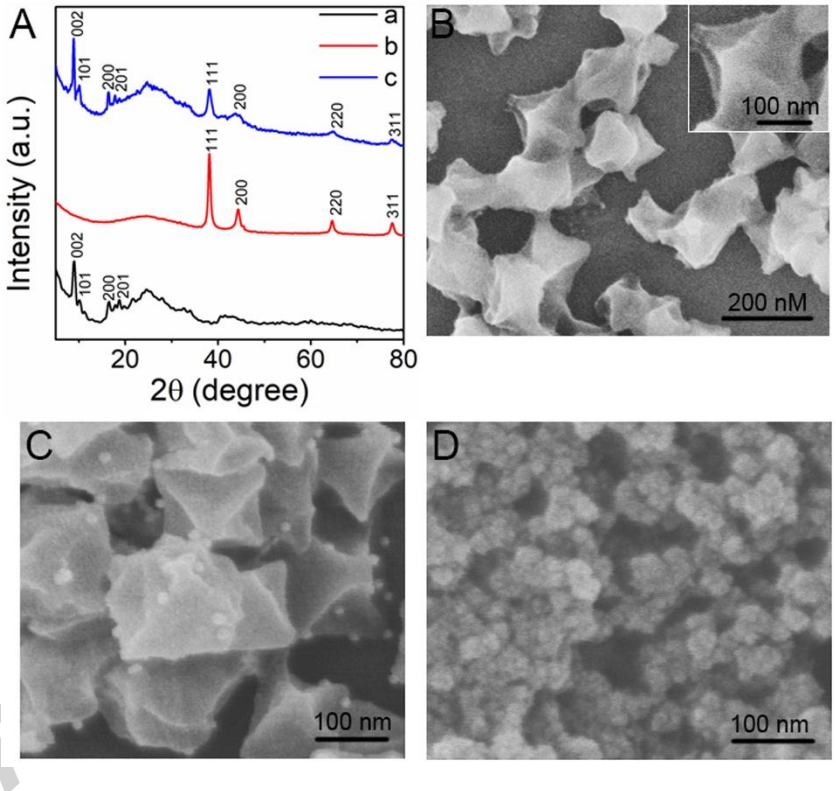

Fig. 1 (A) XRD patterns of the FeMOF (a), AuNPs (b), and FeMOF@AuNPs (c). (B-D) SEM images of FeMOF (B), FeMOF@AuNPs (C), and prussian blue films prepared from the FeMOF@AuNPs (D). Inset in B shows the enlarged SEM image of FeMOF. The scale bar is 100 nm.

3.3. Simulated Assay

The effect of H^+ was simulated by externally adding HCl to the reaction solution, as recorded by digital photo (**Fig. 2A**). The FeMOF is well dispersed in water to form a homogeneous suspension with brown color (**Fig. 2A, a**). The mixture of $K_4Fe(CN)_6$ and HCl (**Fig. 2A, b**) results in clear and colorless. In contrast, the mixture of HCl and FeMOF with $K_4Fe(CN)_6$ leads to blue color (**Fig. 2A, c**), indicating the formation of prussian blue ($Fe_4[Fe(CN)_6]_3$). The prussian blue products generated from the FeMOF are further confirmed by CV (**Fig. 2B**). The CV response of the FeMOF-modified GCE presents a pair of strong characteristic redox peaks at 0.2 V (**Fig. 2B, black curve**), corresponding to the reduction/oxidation of a high-spin system $Fe^{3+}/^{2+}$ in prussian blue ($KFe^{III}Fe^{II}(CN)_6$). The reduction and oxidation reactions of soluble prussian blue may be described as follows (Koncki 2002):

$$KFe^{III}Fe^{II}(CN)_6 + e^- + K^+ \longrightarrow K_2Fe^{III}Fe^{II}(CN)_6 \qquad (1)$$

$$KFe^{III}Fe^{II}(CN)_6 \longrightarrow Fe^{III}Fe^{II}(CN)_6 + e^- + K^+ \qquad (2)$$

The formal potential ($E' = (E_{pa} + E_{pc})/2$), the mean values of the anodic and cathodic peak potentials, are determined to be + 0.147 V and + 0.142 V versus SCE with peak separation ($\Delta E_p = E_{pa} - E_{pc}$) of 37 mV and 18 mV at scan rate of 50 mV s^{-1} and 10 mV s^{-1} (**Supplementary information, Fig. S3**), respectively. The peak separation is close to 0 mV, which should be ideally observed for an adsorbed electroactive species on the electrode surface with a facile electron transfer (Haghighi et al. 2010). In contrast, the absence of the FeMOF leads to CV curves without any peak (**Fig. 2B, red curve**), indicating no prussian blue formation due to the lack of Fe^{3+} source without the FeMOF.

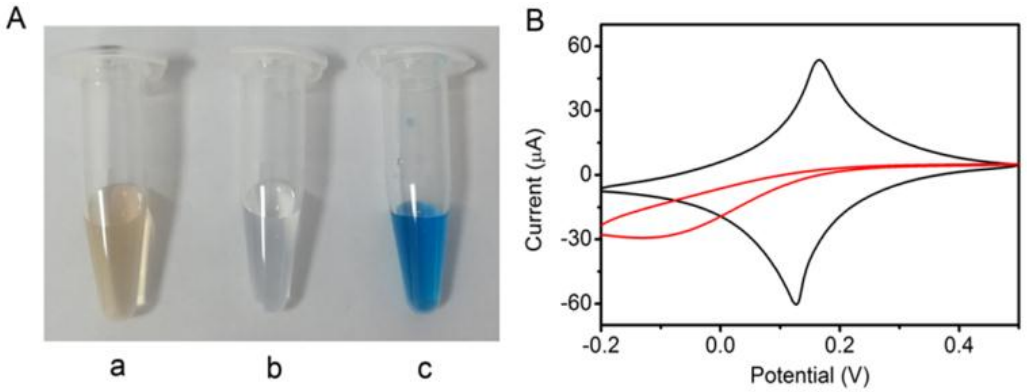

Fig. 2 (A) Digital photo of (a) the FeMOF (0.1 mg mL^{-1}) (b) HCl + $K_4Fe(CN)_6$, and (c) HCl + FeMOF + $K_4Fe(CN)_6$. The 0.4 mM $K_4Fe(CN)_6$, 0.1 M HCl, and 1 mg·mL^{-1} FeMOF were used in the experiments. (B) CV curves of the FeMOF-modified GCE in the absence (red) and presence (black) of reaction solution containing 0.5 mM $K_4Fe(CN)_6$ and 0.1 M KCl. The scan rate is 50 mV·s^{-1}.

3.4. Electrochemical Characterization of Different Modified Electrodes

The electrochemical impedance spectra (EIS) were used for interfacial study (**Supplementary information, Fig. S2)**. In addition, we investigated the CV curves of prussian blue obtained by incubating the FeMOF@AuNPs-hairpin probe with the MCH/capture probe/AuNPs/chitosan/GCE in the presence of PNK, ATP and lambda exonuclease at different scan rates **(Supplementary information, Fig. S3)**.

3.5. CV Response and Calibration Curves

The sensitivity of the electrochemical sensor was studied by cyclic voltammetric measurement. Under the optimally experimental conditions **(Supplementary information, Fig. S4)**, the anodic and cathodic peak currents enhance with the increasing concentration of PNK (**Fig. 3A**). Two linear relationships are obtained

between the peak current and the logarithm of PNK concentration from 0.0005 to 10 U mL^{-1} (**Fig. 3B**). The correlation equations are I_{pa} = 2.008 $\log_{10} C$ + 7.345 (R^2 = 0.9974) and I_{pc} = -2.139 $\log_{10} C$ — 7.934 (R^2 = 0.9967), where I_{pa} and I_{pc} are anodic and cathodic peak current of the electrochemical sensor in the presence of PNK, respectively, and C is the concentration of PNK. The detection limit of the electrochemical sensor is calculated to be 2.344 × 10^{-4} U mL^{-1} using anodic peak current and 2.884 × 10^{-4} U mL^{-1} using cathodic peak current. These two detection limits are closed with each other, suggesting that the reversible radox signal of prussian blue can be used for electrochemical biosensing. Notably, this method exhibits ultrahigh sensitivity superior to most existing assays (**Supplementary information, Table S2**), with at least 5.3-fold higher than that of bioluminescent assay (Du et al. 2014), 2.7-fold higher than those of the reported electrochemical methods (Cui et al. 2018; Wang et al. 2014; Lin et al. 2013; Miao et al. 2011; Peng et al. 2013; Zhang et al. 2015; Zhang et al. 2016), 6.2-fold higher than those of colorimetric methods (Jiang et al. 2013, 2014), 3.5-fold higher than those of fluorescent method (Feng et al. 2018; Hou et al. 2014; Jiao et al. 2012; Lin et al. 2011; Ma et al. 2013; Song et al. 2015; Zhou et al. 2015), and 3.5-fold higher than that of photoelectronchemical method (Zhuang et al. 2015). The ultrahigh sensitivity can be attributed to (1) the specific PNK-mediated phosphorylation, and the efficient cleavage of phosphorylated hairpin probe by lambda exonuclease, (2) the excellent electroactivity of FeMOF for signal amplification, (3) the self-sacrificial label of FeMOF induces the formation of prussian blue nanolayers on the electrode surface with good electrochemical activity, and (4) the extremely low electrochemical background in the absence of target.

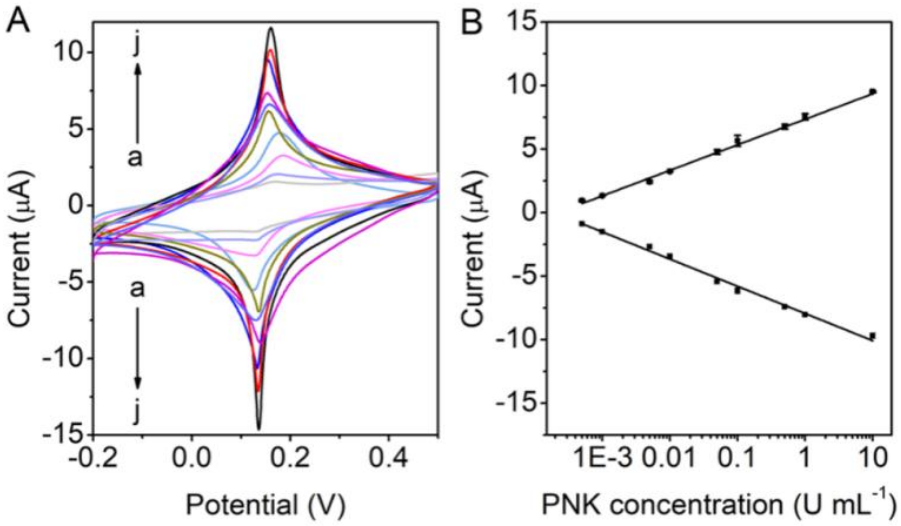

Fig. 3 (A) Measurement of CV current of the electrochemical biosensor in response to different-concentration PNK (from a to j: 0, 0.0005, 0.001, 0.005, 0.01, 0.05, 0.1, 0.5, 1, 10 U mL^{-1}). (B) The linear relationship between the peak current and the logarithm of PNK concentration. The ATP concentration is 0.7 mM, and the amount of lambda exonuclease is 10 U. The error bars represent the standard deviation of three independent experiments.

3.6. Detection Specificity

To investigate the specificity of the proposed method, we used the heat-inactivated T4 PNK and some irrelevant proteins including PKA, lysozyme, T4 DNA ligase, E. coli ligase and BSA as the interferences. Only PNK can induce the increase of anodic and cathodic peak currents significantly (**Fig. 4**). In contrast, the two peak current responses remain unchanged in the presence of irrelevant proteins and the heat-inactivated T4 PNK. This can be explained by the fact that BSA, lysozyme, T4 DNA ligase and E. coli ligase cannot catalyze the transfer of gamma-phosphate group of ATP to the 5′-hydroxyl termini of nucleic acids (Jiang et al. 2014; Tao et al. 2015). E. coli ligase and T4 DNA ligase have ligase activity,

but E. coli ligase needs the cofactor of nicotinamide adenine dinucleotide (NAD^+) and T4 DNA ligase needs the cofactor of adenosine triphosphate (ATP) (Jiang et al. 2014). The PKA can only catalyze the transfer of phosphate from gamma position of ATP to serine hydroxyl group of the substrate peptides (Hu et al. 2017). These results clearly indicate the good specificity of the proposed method for PNK assay.

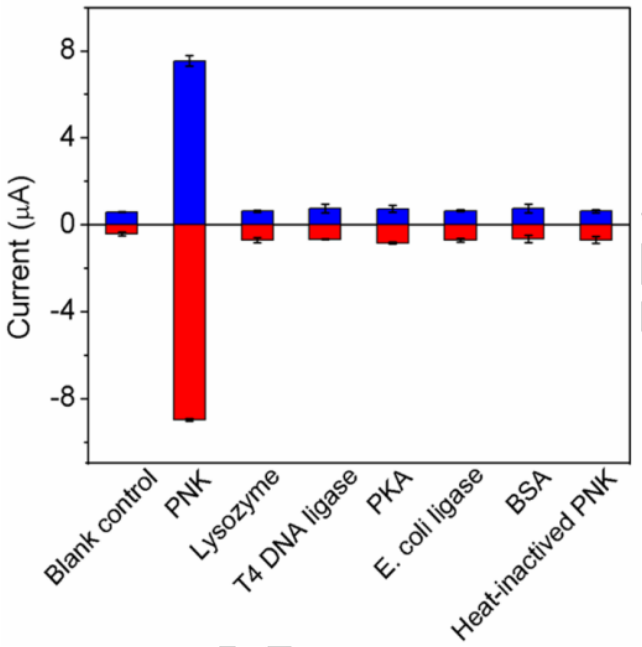

Fig. 4 Specificity of the electrochemical biosensor for PNK assay. The 1 U mL^{-1} PNK, 10 μM Lysozyme, 100 U mL^{-1} T4 DNA ligase, 100 U mL^{-1} PKA, 100 U mL^{-1} E. coli ligase, 10 μM BSA, 1 U mL^{-1} heat-inactivated T4 PNK were used in the experiments. Error bars represent the standard deviation of three independent experiments.

3.7. PNK Inhibitor Assay

PNK is closely associated with various human diseases (Shen et al. 2010) and may function as a potential target in the radio-therapeutic treatment of somatic cancers (Allinson 2010). Thus, the screening of effective inhibitors is crucial to the

PNK-related cancer diagnosis and therapy. We used ADP, Na_2HPO_4 and $(NH_4)_2SO_4$ as the model inhibitors to investigate the feasibility of the proposed method for PNK inhibition assay. As shown in **Fig. 5A**, both the anodic and cathodic peak currents decrease with the increase of ADP concentration, indicating the inhibition of DNA phosphorylation by ADP. The coexistence of ADP and 5′-phosphoryl nucleic acids in the reaction buffer may cause the reversible phosphorylation reaction (Tang et al. 2005). The half maximal inhibition value (IC_{50}) of ADP is calculated to be 1.35 mM, consistent with that obtained by the nanochannel-based electrochemical method (1 mM) (Lin et al. 2013). The high-concentration salts (Na_2HPO_4 and $(NH_4)_2SO_4$) may induce the conformational change of PNK enzyme (Lillehaug and Kleppe 1975), leading to efficient inhibition of PNK activity. As shown in **Fig. 5B and 5C**, both the anodic and cathodic peak currents decrease with the increasing concentration of Na_2HPO_4 and $(NH_4)_2SO_4$, respectively. The IC_{50} value is calculated to be 24.3 mM for Na_2HPO_4 and 10.5 mM for $(NH_4)_2SO_4$, respectively, consistent with those obtained by the AuNP-mediated cleavage-based electrochemical method (23 mM for Na_2HPO_4) (Cui et al. 2018) and the graphene oxide-based fluorescent method (10 mM for $(NH_4)_2SO_4$) (Lin et al. 2011). These results demonstrate that the proposed method can be used to screen the PNK inhibitors for drug discovery. In addition, this electrochemical biosensor exhibits good stability and reproducibility (**Supplementary information, Fig. S5)**.

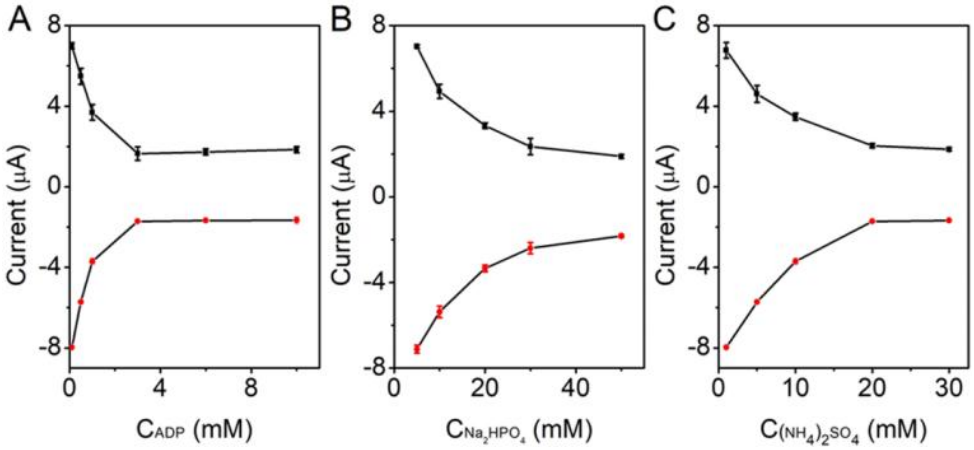

Fig. 5 Variance of anodic and cathodic peak currents with the concentration of ADP (A), Na_2HPO_4 (B), and $(NH_4)_2SO_4$ (C). The error bars represent the standard deviation of three independent experiments.

3.8. Real Sample Analysis

To investigate the capability of the proposed method for real sample analysis, we measured the PNK activity in Hela cell lysate. Both the anodic and cathodic peak currents increase with the logarithm of PNK concentration from 0.05 to 10 U mL^{-1}, and the correlation equation is $I_{pa} = 2.088 \log_{10} C + 4.295$ ($R^2 = 0.9968$) and $I_{pc} = -2.5067 \log_{10} C - 4.767$ ($R^2 = 0.9926$), respectively, where C represents the PNK concentration, I_{pa} and I_{pc} are anodic and cathodic peak currents, respectively (**Supplementary information, Fig. S6**). The detection limit is calculated to be 9.311×10^{-3} using anodic current and 9.804×10^{-3} U mL^{-1} using cathodic current. These results indicate the capability of this method for accurate quantification of PNK in complex samples.

4. Conclusions

In summary, we have developed for the first time a new electrochemical biosensor for signal-on detection of PNK based on the enhanced quasi-reversible redox signal of prussian blue generated by self-sacrificial label of FeMOF. This electrochemical biosensor can be simply fabricated and exhibits high sensitivity with a detection limit of as low as 2.344×10^{-4} using anodic peak current and 2.884×10^{-4} U mL^{-1} using cathodic peak current and a large dynamic range from 0.0005 to 10 U mL^{-1}, which is superior to the reported electrochemical, photoelectrochemical, colorimetric and fluorescent methods for PNK assay (Cui et al. 2018; Jiang et al. 2014; Zhou et al. 2015; Zhuang et al. 2015). Notably, this electrochemical biosensor has distinct advantages: (1) the detection of prussian blue signal is a signal-on measurement, which can avoid the false positivity and improves the accuracy; (2) this assay uses the self-sacrificial label of FeMOF to achieve great signal amplification without the involvement of any extra functional materials; (3) this assay avoids the use of the pre-synthesized prussian blue which is unstable in neutral buffer. Importantly, this method can be used to characterize the PNK inhibitors and can be extended to detect other kinases through the design of appropriate DNA/peptide substrates, holding great potential for further applications in biological researches, clinic diagnosis, and drug development.

Author Contributions

† These authors contributed equally.

Acknowledgments

This work was supported by the National Natural Science Foundation of China (Grant Nos. 21325523, 21527811, 21735003 and 21605096), and the Award for Team Leader Program of Taishan Scholars of Shandong Province, China.

References

Ai, L., Li, L., Zhang, C., Fu, J., Jiang, J., 2013. Chem. Eur. J. 19, 15105-15108.

Allinson, S.L., 2010. Future Oncol. 6, 1031-1042.

Ambrosi, A., Castaneda, M.T., Killard, A.J., Smyth, M.R., Alegret, S., Merkoci, A., 2007. Anal. Chem. 79, 5232-5240.

Bi, W., Zhou, M., Ma, Z., Zhang, H., Yu, J., Xie, Y., 2012. Chem. Commun. 48, 9162-9164.

Breslin, C., Caldecott, K.W., 2009. Molecul. Cell. Biol. 29, 4653-4662.

Brosh, R., Bohr, V., 2007. Nucleic Acids Res. 35, 7527.

Chen, W.S., Zeng, K., Liu, H., Ouyang, J., Wang, L.Q., Liu, Y., Wang, H., Deng, L., Liu, Y.N., 2017. Adv. Funct. Mater. 27, 1605795.

Cui, F., Deng, Q., Sun, L., 2015a. RSC Adv. 5, 98215-98221.

Cui, L., Li, Y., Lu, M., Tang, B., Zhang, C.-Y, 2018. Biosens. Bioelectron. 99, 1-7.

Cui, L., Wu, J., Ju, H., 2014. ACS Appl. Mater. Interfaces 6, 16210-16216.

Cui, L., Wu, J., Li, J., Ju, H., 2015b. Anal. Chem. 87, 10635-10641.

Cui, L., Zhu, J. Y., Meng, X. M., Yin, H. S., Pan, X. P., Ai, S. Y., 2012. Sens. Actuators B Chem. 161, 641-647.

Ding, B., Wang, J., Chang, Z., Xu, G., Hao, X., Shen, L., Dou, H., Zhang, X., 2016. Chemelectrochem 3, 668-674.

Du, J., Xu, Q., Lu, X., Zhang, C., 2014. Anal. Chem. 86, 8481-8488.

Feng, C., Wang, Z., Chen, T., Chen, X., Mao, D., Zhao, J., Li, G., 2018. Anal. Chem. 90, 2810-2815.

Feng, D.W., Gu, Z.Y., Li, J.R., Jiang, H.L., Wei, Z.W., Zhou, H.C., 2012. Angew. Chem. Int. Ed. 51, 10307-10310.

Furukawa, H., Cordova, K.E., O'Keeffe, M., Yaghi, O.M., 2013. Science 341,

1230444.

Wang.G. F., Chen. L., He. X. P., Zhu Y. H., Zhang. X. J., 2014. Analyst 139, 3895-3900.

Haghighi, B., Hamidi, H., Gorton, L., 2010. Sens. Actuators B Chem. 147, 270-276.

Horcajada, P., Surble, S., Serre, C., Hong, D.Y., Seo, Y.K., Chang, J.S., Greneche, J.M., Margiolaki, I., Ferey, G., 2007. Chem. Commun. 2820-2822.

Hou, T., Wang, X., Liu, X., Lu, T., Liu, S., Li, F., 2014. Anal. Chem. 86, 884.

Hu, J., Li, Y., Li, Y., Tang, B., Zhang, C.-Y., 2017. Anal. Chem. 89, 12992-12999.

Jiang, C., Yan, C., Jiang, J., Yu, R., 2013. Anal. Chim. Acta 766, 88-93.

Jiang, H.X., Kong, D.M., Shen, H.X., 2014. Biosens. Bioelectron. 55, 133-138.

Jiang, Z., Gao, P., Yang, L., Huang, C., Li, Y., 2015. Anal. Chem. 87, 12177.

Jiao, H., Wang, B., Jian, C., Liao, D., Li, W., Cong, Y., 2012. Chem. Commun. 48, 7862-7864.

Koncki, R., 2002. Crit. Rev. Anal. Chem. 32, 79-96.

Kong, B., Selomulya, C., Zheng, G., Zhao, D., 2015. Chem. Soc. Rev. 44, 7997-8018.

Lai, G., Yan, F., Ju, H., 2009. Anal. Chem. 81, 9730-9736.

Li, J., Li, Y., Zhang, Y., Wei, G., 2012. Anal. Chem. 84, 1888-1893.

Li, K.W., Lima, C.D., Shuman, S., 2014a. Embo J. 21, 3873-3880.

Li X., Zhu, L.S., Zhou, Y. L., Yin, H. S., Ai, S. Y., 2017. Analytical Chemistry 89, 2369-2376.

Li, Y., Xu, M., Li, P., Dong, J., Ai, S.Y., 2014b. Anal. Methods 6, 2157-2162.

Lillehaug, J.R., Kleppe, K., 1975. Biochemistry 14, 1225-1229.

Lin, L., Liu, Y., Yan, J., Wang, X., Li, J., 2013. Anal. Chem. 85, 334-340.

Lin, L., Liu, Y., Zhao, X., Li, J., 2011. Anal. Chem. 83, 8396-8402.

Liu, J., Chen, L., Cui, H., Zhang, J., Zhang, L., Su, C.Y., 2014. Chem. Soc. Rev. 43,

6011-6061.

Liu, Y. L., Zhao, X. J., Yang, X. X., Li, Y. F., 2013. Analyst 138, 4526-4231.

Ma, C., Fang, H., Wang, K., Xia, K., Chen, H., He, H., Zeng, W., 2013. Anal. Biochem. 443, 166-168.

McKinlay, A.C., Eubank, J.F., Wuttke, S., Xiao, B., Wheadey, P.S., Bazin, P., Lavalley, J.C., Daturi, M., Vimont, A., De Weireld, G., Horcajada, P., Serre, C., Morris, R.E., 2013. Chem. Mater. 25, 1592-1599.

Miao, P., Ning, L., Li, X., Shu, Y., Li, G., 2011. Biosens. Bioelectron. 27, 178.

Orellana-Tavra, C., Baxter, E.F., Tian, T., Bennett, T.D., Slater, N.K., Cheetham, A.K., Fairen-Jimenez, D., 2015. Chem. Commun. 51, 13878.

Peng, Y., Jiang, J., Yu, R., 2013. RSC Adv. 3, 18128-18133.

Rasouli-Nia, A., Karimi-Busheri, F., Weinfeld, M., 2004. P. Natl. Acad. Sci USA 101, 6905-6910.

Ricci, F., Amine, A., Palleschi, G., Moscone, D., 2003. Biosens. Bioelectron. 18, 165-174.

Sarkar, S., Bhattacharjee, K., Das, G.C., Chattopadhyay, K.K., 2014. CrystEngComm 16, 2634-2644.

Sharma, S., Doherty, K.M., Jr, B.R., 2006. Biochem. J. 398, 319-337.

Shen, J., Gilmore, E.C., Marshall, C.A., Haddadin, M., Reynolds, J.J., Eyaid, W., Bodell, A., Barry, B., Gleason, D., Allen, K., Ganesh, V.S., Chang, B.S., Grix, A., Hill, R.S., Topcu, M., Caldecott, K.W., Barkovich, A.J., Walsh, C.A., 2010. Nat. Genet. 42, 245-249.

Shen, W.J., Zhuo, Y., Chai, Y.Q., Yuan, R., 2015. Anal. Chem. 87, 11345-11352.

Song, C., Yang, X., Wang, K., Wang, Q., Liu, J., Huang, J., He, L., Liu, P., Qing, Z., Liu, W., 2015. Chem. Commun. 51, 1815-1818.

Su, S., Han, X., Lu, Z., Liu, W., Zhu, D., Chao, J., Fan, C., Wang, L., Song, S., Weng, L., 2017. ACS Appl. Mater. Interfaces 9, 12773-12781.

Su, Y.Y., Teng, Z., Yao, H., Wang, S.J., Tian, Y., Zhang, Y.L., Liu, W.F., Tian, W., Zheng, L.J., Lu, N., Ni, Q.Q., Su, X.D., Tang, Y.X., Sun, J., Liu, Y., Wu, J., Yang, G.F., Lu, G.M., Zhang, L.J., 2016. ACS Appl. Mater. Interfaces 8, 17038-17046.

Surble, S., Serre, C., Mellot-Draznieks, C., Millange, F., Ferey, G., 2006. Chem. Commun. 284-286.

Tang, Z., Wang, K., Tan, W., Ma, C., Li, J., Liu, L., Guo, Q., Meng, X., 2005. Nucleic Acids Res. 33, e97-e97.

Tao, M., Shi, Z., Cheng, R., Zhang, J., Li, B., Jin, Y., 2015. Anal. Biochem. 485, 18-24.

Taylor-Pashow, K.M., Della Rocca, J., Xie, Z., Tran, S., Lin, W., 2009. J. Am. Chem. Soc. 131, 14261-14263.

Wang, M., Fu, Z. L., Li, B. C., Zhou, Y. L., Yin, H. S., Ai, S. Y., 2014. Anal. Chem. 86, 5606-5610.

Wang, M., Yang, L., Hu, B., Liu, J., He, L., Jia, Q., Song, Y., Zhang, Z., 2018. Biosens. Bioelectron. 113, 16-24.

Whitehouse, C.J., Taylor, R.M., Thistlethwaite, A., Zhang, H., Karimibusheri, F., Lasko, D.D., Weinfeld, M., Caldecott, K.W., 2001. Cell 104, 107-117.

Wiederhold, L., Leppard, J.B., Kedar, P., Karimi-Busheri, F., Rasouli-Nia, A., Weinfeld, M., Tomkinson, A.E., Izumi, T., Prasad, R., Wilson, S.H., 2004. Molecular Cell 15, 209-220.

Yin, H. S., Yang, Z. Q., Li, B., Zhou, Y. L., Ai, S. Y., 2015. Biosens. Bioelectron. 66, 266-270.

Zhang, J.W., Zhang, H.T., Du, Z.Y., Wang, X., Yu, S.H., Jiang, H.L., 2014. Chem.

Commun. 50, 1092-1094.

Zhang, Q., Li, L., Qiao, Z., Lei, C., Fu, Y., Xie, Q., Yao, S., Li, Y., Ying, Y., 2017. Anal. Chem. 89, 12145-12151.

Zhang, Q., Li, X., Li, B., Yin, H., Ai, S. Y., 2015. Anal. Methods 7, 9984-9991.

Zhang, Q. M., Li, Z., Zhou, Y. L., Li, X., Li, B., Yin, H. S., Ai, S. Y., 2016. Sens. Actuators B Chem.225, 151-157.

Zhou, L., Shen, X., Sun, N., Wang, K., Zhang, Y., Pei, R., 2015. Analyst 140, 5450.

Zhou, S., Wei, Y., Hou, J., Ding, L.-X., Wang, H., 2017. Chem. Mater. 29, 7103-7107.

Zhuang, J., Lai, W., Xu, M., Zhou, Q., Tang, D., 2015. ACS Appl Mater Interfaces 7, 8330-8338.

Zou, F., Hu, X., Li, Z., Qie, L., Hu, C., Zeng, R., Jiang, Y., Huang, Y., 2014. Adv. Mater. 26, 6622-6628.

Highlights

- We develop a new electrochemical biosensor for signal-on detection of T4 polynucleotide kinase (PNK).
- This electrochemical biosensor is based on the enhanced quasi-reversible redox signal of prussian blue generated by self-sacrificial label of iron metal-organic framework (FeMOF).
- This assay is very simple without the involvement of the pre-synthesized prussian blue which is unstable in neutral buffer.
- The self-sacrificial label of FeMOF can achieve great signal amplification without the involvement of any extra functional materials.